Strain-Enhanced Charge-to-Spin Conversion in Ta/Fe/Pt Multilayers Grown on Flexible Mica Substrate

Er Liu, T. Fache, D Cespedes-Berrocal, Zhi Zhang, S. Petit-Watelot, Stéphane Mangin, Feng Xu, J.-C Rojas-Sánchez

Strain-Enhanced Charge-to-Spin Conversion in Ta/Fe/Pt Multilayers Grown on Flexible Mica Substrate

Er Liu,[1,2,*] T. Fache,[2] D. Cespedes-Berrocal,[2,3] Zhi Zhang,[1] S. Petit-Watelot,[2] Stéphane Mangin,[2] Feng Xu,[1,†] and J.-C. Rojas-Sánchez[2,‡]

[1] *MIIT Key Laboratory of Advanced Metallic and Intermetallic Materials Technology, School of Materials Science and Engineering, Nanjing University of Science and Technology, Nanjing 210094, China*

[2] *Université de Lorraine, CNRS UMR 7198, Institut Jean Lamour, F-54011 Nancy, France*

[3] *Universidad Nacional de Ingeniería, Rímac 15333, Peru*

(Received 1 August 2019; revised manuscript received 17 September 2019; published 31 October 2019)

Recent demonstration of magnetization manipulation has been focused on the utilization of pure spin current converted by charge current in nonmagnetic materials with strong spin-orbit coupling (SOC), which stimulates intensive studies on the exploration of materials with larger SOC, such as heavy metals and topological insulators. We suggest an alternative approach for enhancing the effective charge-to-spin conversion efficiency by applying strain in Ta/Fe/Pt films grown on flexible mica substrates. We experimentally demonstrate a large and tunable charge-to-spin conversion efficiency in Ta/Fe/Pt films by applying compressive strain within a flexible substrate, and over 50% enhancement of effective spin Hall angle Θ_{SHE}^{eff} of up to approximately 0.2 is achieved in a 6.26‰ strained film. Our findings may spur further work on the integration of flexible electronics and SOC and may potentially lead to the innovation of alternative flexible spintronics devices.

DOI: 10.1103/PhysRevApplied.12.044074

I. INTRODUCTION

The integration of an electronic system with a flexible substrate has received considerable attention due to the appealing applications in alternative devices such as flexible display, electronic skin, and wearable devices [1–5]. The fantastic property of such flexible electronics also triggers numerous research efforts in the spintronics field on the flexible strain effects of spin-dependent phenomena such as exchange bias [6,7], interlayer coupling [8], and perpendicular magnetic anisotropy (PMA) [9]. In recent years, the focus of modern spintronics has been shifted to the generation and manipulation of pure spin currents through spin-orbit coupling (SOC) in nonmagnetic systems [10–12], the studies of which even give birth to an emerging field, that is, spin orbitronics [13]. However, the integration of pure spin currents in flexible electronics remains largely unexplored.

As a flow of angular momentum that does not accompany a charge flow, pure spin currents carry information with minimum power dissipation [14]. More importantly, similar to spin-polarized current, pure spin currents are capable of manipulating the magnetization of ferromagnetic elements, showing promising application perspectives in alternative information recording and data processing devices such as spin orbital torque magnetic random access memory (SOT MRAM) [15] and spin Hall nano-oscillators [16]. In a ferromagnetic-nonmagnetic (FM NM) bilayer system, pure spin currents can be converted by charge current flowing through NM with strong spin orbit coupling (spin Hall effect), then propagate into the adjacent FM, thereby affecting the magnetic fluctuation, magnetization dynamics, and even magnetization switching [17–19]. In consideration of the FM-NM interface spin loss during the injection of spin currents, the effective charge-to-spin conversion is quantified by the effective spin Hall angle Θ_{SHE}^{eff} [20,21]. As such, optimizing the effective spin Hall angle Θ_{SHE}^{eff} for specific applications is of immense importance and has been achieved by various strategies, including exploring NM with large spin orbital coupling such as heavy metals [18,20,22,23], topological insulators [19,24] and more recently, the antiferromagnetic material [25,26], engineering the FM-NM interface for greater spin transparency [27], or reducing interfacial spin memory loss [20]. Here, we report the observation of a large and tunable Θ_{SHE}^{eff} in mica//Ta/Fe/Pt by applying mechanical strain in a flexible mica substrate during film deposition.

*ericliu@njust.edu.cn

†xufeng@njust.edu.cn

‡juan-carlos.rojas-sanchez@univ-lorraine.fr

II. EXPERIMENTAL PROCEDURES

A. Film deposition

A series of Ta(4 nm)/Fe (4 nm)/Pt(5 nm) multilayers are deposited on flexible mica substrates, with the 4-nm Ta employed as a buffer layer to reduce the roughness of the flexible substrates. Before the deposition, the substrates are cleaned with ethyl alcohol in an ultrasonic cleaner for 10 min and then dried with nitrogen gas. During the deposition, the substrates are bent and fixed on a home-made convex aluminum alloy mold, as shown in Fig. 1(a). Thus, a longitudinal compressive strain is induced in the films when flattening the substrate after the deposition and the strain direction is shown in Fig. 1(b). By changing the curvature radii of the mold, Ta/Fe/Pt multilayers with compressive strain ε of 0 to approximately 6.26‰ are obtained. The magnitude of such induced strains is estimated by $\varepsilon = T/2R$, where R is the curvature radii of the mold and T is the total thickness including both the substrate and multilayers [28].

B. Device fabrication

The microstrips for measurements are patterned with the long axis parallel to the strain directions by standard UV lithography and have lateral sizes of $20 \times 90\ \mu m^2$. Ti/Au electrodes are deposited on the edge of the microstrip by the lift-off technique to form a ground-signal-ground (GSG) contact that guides the radio frequency (rf) current into the sample. We also prepare a control sample with the long axis perpendicular to the strain direction for the multilayer with a compressive strain of 6.26‰.

III. RESULTS AND DISCUSSION

A. ST FMR measurements

Spin-torque ferromagnetic resonance (ST FMR), [also referred to as spin-orbit ferromagnetic resonance, that is, SO FMR)] [22,29] measurements are performed to evaluate the efficiency of charge-to-spin conversion for all the microstrip devices, and the schematic of the measurement setup is illustrated in Fig. 1(c). A rf charge current J_c with a power of 10 dBm is injected into the microstrip in the presence of an external field H that is applied in plane at 45° with respect to the microstrip, as shown in Fig. 1(d). Note that for all the measurements, the rf current is flowing along the long axis of the microstrip devices with a frequency ranging from 5–20 GHz. A transverse spin current is then converted by the rf current in Pt due to the spin Hall effect, which manipulates the magnetization procession of Fe by exerting two orthogonal torques, namely, a dampinglike torque (τ_D) and a fieldlike torque (τ_F). Owing to the anisotropic magnetoresistance (AMR) effect, the oscillating magnetization gives rise to a time-dependent resistivity, which mixes with the rf current and results in a rectified dc voltage.

Figure 2(a) shows the dc voltage signal for a Ta/Fe/Pt device with compressive strain of 6.26‰, measured by spin-torque ferromagnetic resonance under a configuration of $J_c || \varepsilon$. It is notable that the resonance field shifts toward higher fields as the rf current frequency increases, which is consistent with the Kittel model [30]. Here, the measured dc voltages are a mixture of a symmetric Lorentzian component V_{sym} due to the dampinglike torque and an antisymmetric one V_{anti} arising from the fieldlike torque,

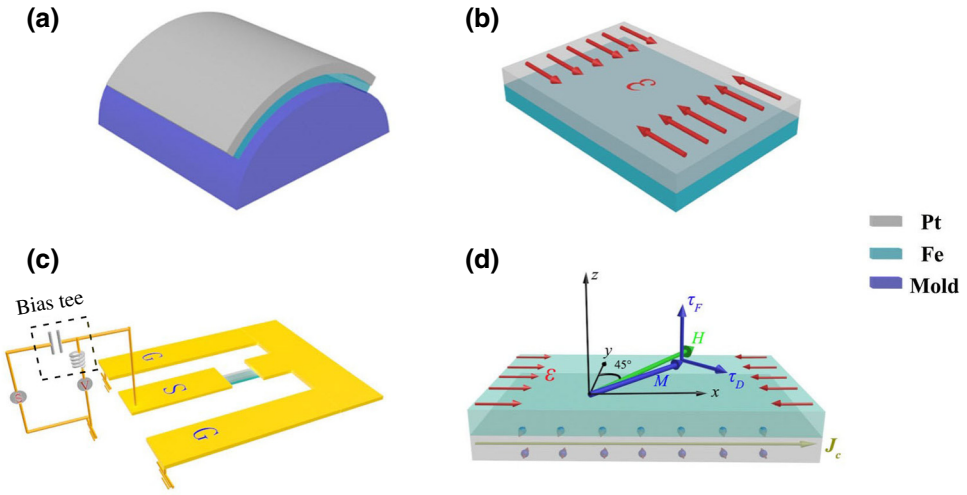

FIG. 1. (a),(b) Schematic illustration of the strain application process. The fix of mica on a convex aluminum alloy mold during the film deposition and the flattening afterward induced a compressive strain ε in the films with direction shown in (b). (c) Schematic representation of the ST FMR experimental setup. (d) Sketch of the ST FMR experimental configuration showing the spin-transfer torques τ_F and τ_D, magnetization M, and external field H. Here, the charge current J_c is parallel to the strain ε direction.

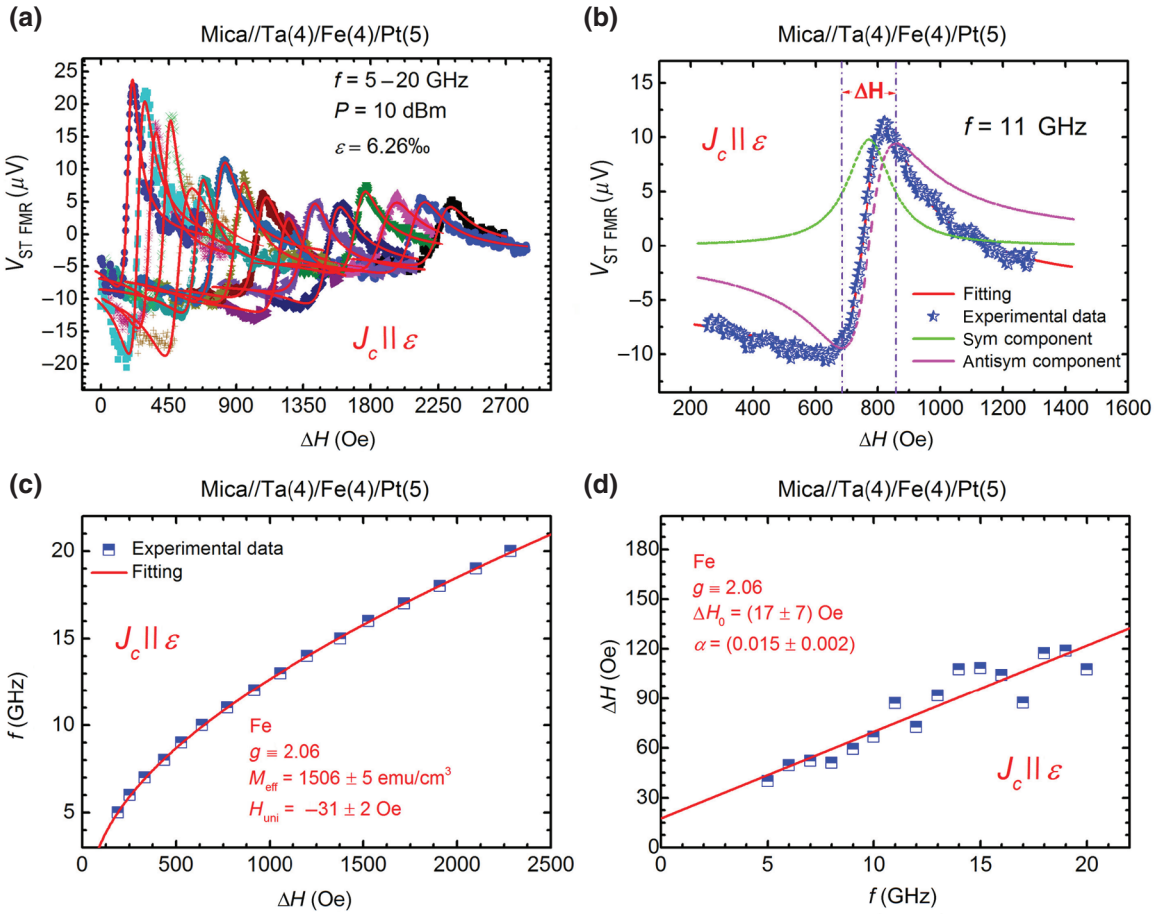

FIG. 2. ST FMR data for the 6.26‰ strained film. (a) The measured ST FMR signals at different frequencies, the red lines are the fittings according to Eq. (1). (b) Single ST FMR spectrum measured at 11 GHz. The red solid line represents the fit to the Lorentzian function. The green and purple dash-dotted lines represent symmetric and antisymmetric voltage components, respectively. (c) The fitting of frequency dependence of the resonance field from which we can obtain the value of M_{eff}. (d) Effective damping determination from the fitting of frequency dependence of the line width.

in a first approximation for the level of thicknesses in our samples [22,31,32]. We extract the symmetric and antisymmetric voltage contributions by fitting the spin-torque ferromagnetic resonance spectra with the following equation, also considering an off-set V_{off} [32]

$$V_{\text{dc}} = V_{\text{off}} + V_{\text{sym}}\frac{\Delta H^2}{\Delta H^2 + (H - H_{\text{res}})^2} + V_{\text{anti}}\frac{(H - H_{\text{res}})\Delta H}{\Delta H^2 + (H - H_{\text{res}})^2}, \quad (1)$$

where H, H_{res}, and ΔH are the applied field, the resonance field, and the resonance line width, respectively. Figure 2(a) shows the fitting result and Fig. 2(b) shows the fitting detail of a ST FMR spectrum measured at a frequency of 11 GHz. Both agree well with the experimental data. We extract the resonance fields and plot them against the resonance frequency f_{res} in Fig. 2(c), in which the resonance field dependence of the frequency can be well fitted by the Kittel formula

$$f_{\text{res}} = \frac{\gamma}{2\pi}[(H_{\text{res}} + H_{\text{uni}})(H_{\text{res}} + 4\pi M_{\text{eff}} + H_{\text{uni}})]^{1/2}, \quad (2)$$

where γ and H_{uni} are the gyromagnetic ratio and the in-plane uniaxial magnetic anisotropy field, respectively. $4\pi M_{\text{eff}} = 4\pi M_s - H_k$ is the effective magnetization, M_s is the saturation magnetization, and H_k is the perpendicular anisotropy field. The value of M_{eff} for all the samples is obtained from the fitting and the strain dependence of M_{eff} and is shown in Fig. 2(c). It is notable that M_{eff} slightly increases with the increasing of strain regardless of the strain direction, which probably stems from the increase of H_k due to an out-of-plane stretch of the lattice by the in-plane compressive strain.

B. Strain dependence of magnetic damping

The ST FMR measurements also allow us to evaluate the effective magnetic damping α by fitting the

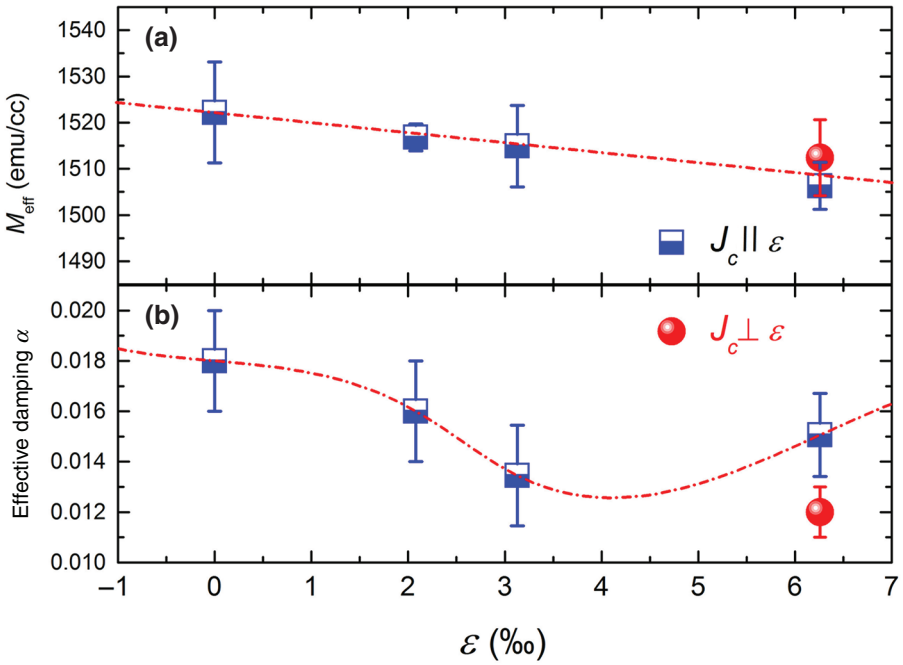

FIG. 3. Strain dependence of M_{eff} (a) and effective damping (b). The dash-dotted lines represent a guide to the eyes. The red circle data point corresponds to the control device where J_c is perpendicular to ε. We can observe in (a) that M_{eff} is the same in both devices for the higher ε we have measured. This is an indication that the Fe layer is isotropic in the film plane. We can observe in (b) that the total damping when J_c is perpendicular to ε is lower than the one with $J_c||\varepsilon$. This is an indication of a more efficient spin pumping contribution when $J_c||\varepsilon$.

frequency dependence of the resonance line width with equation $\Delta H = \Delta H_0 + 2\pi f\,\alpha/\gamma$, where ΔH_0 is the frequency independent contribution due to the inhomogeneity of the films. A fitting example is shown in Fig. 2(d) and a linear dependence can be observed. Figure 3(b) shows the strain dependence of α. It is interesting to find that rather than the monotonous behavior of M_{eff}, α depends on the strain direction and it decreases first then increases with the increasing of strain for a $J_c||\varepsilon$ configuration. We will explain this anomalous behavior in the discussion of $\Theta_{\text{SHE}}^{\text{eff}}$ below.

C. Strain-enhanced charge-to-spin conversion

The spin Hall angle $\Theta_{\text{SHE}}^{\text{eff}}$ is the ratio of spin current density J_s to the rf current density J_c, which in the simplest model is proportional to the ratio of the symmetric voltage component over the antisymmetric one $V_{\text{symm}}/V_{\text{anti}}$. When the resonance field is larger than the saturation field ($H_{\text{res}} > H_{\text{sat}}$), the precession of magnetization is considered to be uniform, as such $\Theta_{\text{SHE}}^{\text{eff}}$ can be obtained by the following equation [11,22,31,32]

$$\Theta_{\text{SHE}}^{\text{eff}} = \frac{J_s}{J_c} \cong \frac{V_{\text{sym}}}{V_{\text{anti}}} \frac{e\mu_0 M_s t_{\text{Fe}} t_{\text{Pt}}}{\hbar} \left[1 + \frac{4\pi M_{\text{eff}}}{H_{\text{res}}}\right]^{1/2} \times \frac{1}{1 + (H_F/H_{\text{Oe}})}, \tag{3}$$

where μ_0 is the permeability in vacuum and t_{Fe} and t_{Pt} are the thicknesses of the Fe and Pt layers, respectively. The last factor in Eq. (3) takes into account a possible contribution H_F due to fieldlike spin orbit torque and H_{Oe} is the Oersted field arising from the rf current. Here, we ignore the contribution of the Oersted field from the Ta layer due to the small current density in Ta, considering the much larger resistivity in Ta (200 μW cm) than that in Pt (24 μW cm). We have estimated the value of the Oersted field ($H_{\text{Oe}} \sim 1.5$ Oe) and the field due to the fieldlike spin orbit torque ($H_F \sim 0.15$ Oe) in our samples according to the method given by Refs. [31] and [33]. Thus, we can neglect the factor H_F/H_{Oe} in Eq. (3). Figure 4(a) shows the effective spin Hall angles $\Theta_{\text{SHE}}^{\text{eff}}$ for Pt in the Ta/Fe/Pt system without and with a strain of 6.26‰ at varying J_c frequencies from 6 to 20 GHz, from which a significant increase of $\Theta_{\text{SHE}}^{\text{eff}}$ by strain is noted. To further confirm the strain effect on $\Theta_{\text{SHE}}^{\text{eff}}$, we also show the $\Theta_{\text{SHE}}^{\text{eff}}$ comparison derived from the ST FMR measurements with J_c flowing along and perpendicular to the strain direction in Fig. 4(b). It is worth noting that in both cases, Figs. 4(a) and 4(b), the value of $\Theta_{\text{SHE}}^{\text{eff}}$ is increased when $J_c||\varepsilon$ and when the magnitude of ε increases. The strain dependence of $\Theta_{\text{SHE}}^{\text{eff}}$ is shown in Fig. 4(c), indicating the increase of $\Theta_{\text{SHE}}^{\text{eff}}$ from 0.12 ± 0.02 to 0.20 ± 0.02 by the increase of strain when $J_c||\varepsilon$. On the contrary, $\Theta_{\text{SHE}}^{\text{eff}}$ is almost constant ($\Theta_{\text{SHE}}^{\text{eff}} = 0.12 \pm 0.02$ and 0.11 ± 0.02 for $J_c \perp \varepsilon$ and $\varepsilon = 0$, respectively) when J_c is not flowing along strain direction. It should be mentioned that the measured $\Theta_{\text{SHE}}^{\text{eff}}$ is larger compared to that reported previously (around 0.05) [20,22,32], and we ascribe this to the presence of the Ta buffer layer, which has a negative spin Hall angle [17,18] thereby also contributing to the spin current density J_s. Even if we do not consider the thickness of Ta, the calculated "effective" value involves the contribution of Ta. Thus, it explains the large value, approximately 0.12, we obtain in our devices without any strain. Similar enhancements of effective values in trilayers have also

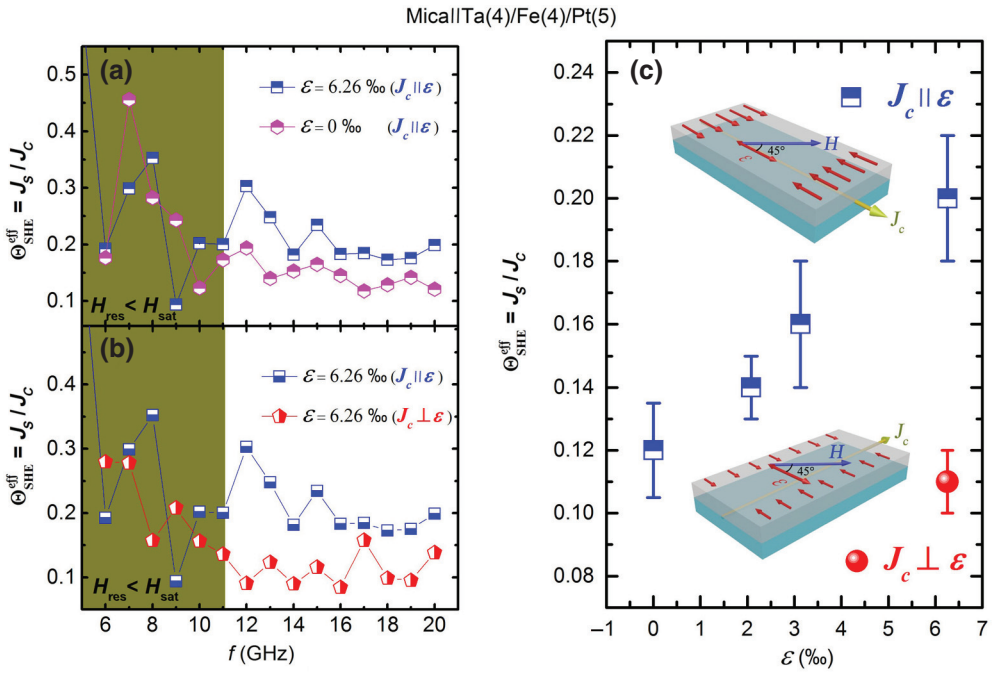

FIG. 4. (a),(b) Determination of the effective spin Hall angle according to Eq. (3), which is reliable only when $H_{res} > H_{sat}$ [32]. (c) Strain dependence of the effective spin Hall angle.

been observed in W/(Co, Fe)B/Pt [31] and Pt/Co/Ta [34] systems.

The strain dependence of Θ_{SHE}^{eff} can also be verified by the anomalous behavior of effective damping α as we mentioned in Fig. 3(b). Here, we consider two damping mechanisms contributing to the effective damping α: one is the intrinsic damping of magnetic layer, which decreases with increasing compressive strain, as reported previously [6]. The other is an additional damping due to spin pumping into the heavy metal, Pt and Ta, layers. Note, however, that the enhancement of damping due to the Ta layer is much smaller than that of Pt [18]. Thus, the clear increase of Θ_{SHE}^{eff} suggests more efficient spin pumping into the heavy metal (HM) layers, thus a larger α for the Fe layer, which agrees with the damping measurements for the two devices with a compressive strain of 6.26‰. Despite the different rf current orientation, the Fe layers in both devices undergo the same magnitude of strain (6.26‰) and magnetic field configuration (H is applied 45° in plane to the strain direction), thus the intrinsic damping of Fe is identical. Consequently, the effective damping is mainly determined by the additional damping due to spin pumping. In contrast, for the devices with different strain, α decreases first then increases with the increase of strain. This can be explained by the competition of strain effect on the intrinsic damping of Fe and the enhancement of spin pumping due to the larger Θ_{SHE}^{eff}.

Finally, we discuss the possible mechanism accounting for the observed strain-dependent Θ_{SHE}^{eff}. It is well known that a magnetoelastic anisotropy will be induced due to strain in the magnetic layer, and in our case, the easy axis of the magnetoelastic anisotropy is in-plane perpendicular to the compressive strain direction [6,28]. However, the observed strain-dependent Θ_{SHE}^{eff} is unlikely due to the strain-induced anisotropy, since different Θ_{SHE}^{eff} are still obtained in the 6.26‰ strained devices in which the same orientation (45°) between the magnetic field and strain direction is given. We note that the variation of $4\pi M_{eff}/H_{res}$ [factor in Eq. (3)] due to strain is less than 1%, thus it cannot account for the 50% variation of the effective spin Hall angle. Moreover, magnetic anisotropy independent Θ_{SHE}^{eff} is also observed in epitaxial Fe/Pt [32] and an exchange-biased NiFe/IrMn system [35]. The increase of SOC in Pt(Ta) is another reason to be ruled out since SOC is dominated by the atomic number of Pt(Ta), which cannot be changed by the strain. A possibility for the strain-dependent Θ_{SHE}^{eff} is the decrease of spin-current dissipation at the interface due to the flexible substrate-induced strain, which may improve the interfacial disorder. More detailed theoretical and experimental investigations are needed to explore the exact microscopic mechanism of the enhanced Θ_{SHE}^{eff} given the complex nature of the system.

IV. CONCLUSION

With the ST FMR technique, we show a large and tunable charge-to-spin conversion efficiency in compressive strained Ta/Fe/Pt films grown on flexible mica substrates, and the effective spin Hall angle Θ_{SHE}^{eff} is significantly enhanced over 50% from 0.12 ± 0.02 to 0.20 ± 0.02 by the flexible substrate-induced strain of 6.26‰. The demonstrated strong strain dependence of charge-to-spin conversion efficiency paves an alternative way for the manipulation of spin current, and we anticipate the results can be

used for the application of alternative spin memory or logic devices as well as the development of flexible electronics.

ACKNOWLEDGMENTS

This work was sponsored by the National Natural Science Foundation of China (Grants No. 51601093, No. 51571121, No. 11604148, and No. 61427812), Fundamental Research Funds for the Central Universities (Grant No. 30916011345), the Natural Science Foundation of Jiangsu Province (Grants No. BK20160833 and No. BK20160831), the China Postdoctoral Science Foundation Funded Project (Grants No. 2015M571285, No. 2016M601811, and No. 2016M591851), the Postdoctoral Science Foundation Funded Project of Jiangsu Province (Grant No. 1601268C), the Key Research & Development Program of Jiangsu Province (Grant No. BE2017102), and Special fund for the transformation of scientific and technological achievements in Jiangsu Province (Grant No. BA2017121). The authors also acknowledge and thank LUE Graduated program internship 2019 from Lorraine Université d'Excellence, the Feder and Region Grand Est for its support in Projet Chercheur d'Avenir, Plateforme Nano-terraHertz and Plus. This work was supported partly by the French PIA project Lorraine Université d'Excellence, No. ANR-15-IDEX-04-LUE. By the ANR-NSF Project, No. ANR-13-IS04-0008-01. Films were grown using equipment from the TUBE – Daum funded by FEDER (EU), ANR, the Region Lorraine, and Grand Nancy. Lithography was performed at the MiNaLor platform.

[1] K. Nomura, H. Ohta, A. Takagi, T. Kamiya, M. Hirano, and H. Hosono, Room-temperature fabrication of transparent flexible thin-film transistors using amorphous oxide semiconductors, Nature **432**, 488 (2004).

[2] J. A. Rogers, T. Someya, and Y. Huang, Materials and mechanics for stretchable electronics, Science **327**, 1603 (2010).

[3] D. Son, J. Kang, O. Vardoulis, Y. Kim, N. Matsuhisa, J. Y. Oh, J. W. F. To, J. Mun, T. Katsumata, Y. Liu, A. F. McGuire, M. Krason, F. Molina-Lopez, J. Ham, U. Kraft, Y. Lee, Y. Yun, J. B.-H. Tok, and Z. Bao, An integrated self-healable electronic skin system fabricated via dynamic reconstruction of a nanostructured conducting network, Nat. Nanotech. **13**, 1057 (2018).

[4] T. Trung and N. Lee, Flexible and stretchable physical sensor integrated platforms for wearable human-activity monitoring and personal healthcare, Adv. Mater. **28**, 4338 (2016).

[5] Y. Guo, M. Zhong, Z. Fang, P. Wan, and G. Yu, A wearable transient pressure sensor made with MXene nanosheets for sensitive broad-range human–machine interfacing, Nano Lett. **19**, 1143 (2019).

[6] Z. Zhang, E. Liu, W. Zhang, P. K. J. Wong, Z. Xu, F. Hu, X. Li, J. Tang, A. T. S. Wee, and F. Xu, Mechanical strain manipulation of exchange bias field and spin dynamics in FeCo/IrMn multilayers grown on flexible substrates, ACS Appl. Mater. Inter. **11**, 8258 (2019).

[7] H. Matsumoto, S. Ota, A. Ando, and D. Chiba, A flexible exchange-biased spin valve for sensing strain direction, Appl. Phys. Lett. **114**, 132401 (2019).

[8] T. Vemulkar, R. Mansell, A. Fernández-Pacheco, and R. P. Cowburn, Toward flexible spintronics: Perpendicularly magnetized synthetic antiferromagnetic thin films and nanowires on polyimide substrates, Adv. Funct. Mater. **26**, 4704 (2016).

[9] S. Zhao, Z. Zhou, C. Li, B. Peng, Z. Hu, and M. Liu, Low-voltage control of (Co/Pt)x perpendicular magnetic anisotropy heterostructure for flexible spintronics, ACS Nano **12**, 7167 (2018).

[10] J. E. Hirsch, Spin Hall Effect, Phys. Rev. Lett. **83**, 1834 (1999).

[11] V. Tshitoyan, C. Ciccarelli, A. P. Mihai, M. Ali, A. C. Irvine, T. A. Moore, T. Jungwirth, and A. J. Ferguson, Electrical manipulation of ferromagnetic NiFe by antiferromagnetic IrMn, Phys. Rev. B **92**, 214406 (2015).

[12] J. Sinova, S. O. Valenzuela, J. Wunderlich, C. H. Back, and T. Jungwirth, Spin Hall effects, Rev. Mod. Phys. **87**, 1213 (2015).

[13] J. C. Rojas Sánchez, L. Vila, G. Desfonds, S. Gambarelli, J. P. Attané, J. M. De Teresa, C. Magén, and A. Fert, Spin-to-charge conversion using Rashba coupling at the interface between non-magnetic materials, Nat. Commun. **4**, 2944 (2013).

[14] X. Tao, Q. Liu, B. Miao, R. Yu, Z. Feng, L. Sun, B. You, J. Du, K. Chen, S. Zhang, L. Zhang, Z. Yuan, D. Wu, and H. Ding, Self-consistent determination of spin Hall angle and spin diffusion length in Pt and Pd: The role of the interface spin loss, Sci. Adv. **4**, eaat1670 (2018).

[15] N. Sato, F. Xue, R. M. White, C. Bi, and S. X. Wang, Two-terminal spin–orbit torque magnetoresistive random access memory, Nat. Electron. **1**, 508 (2018).

[16] H. Mazraati, S. Chung, A. Houshang, M. Dvornik, L. Piazza, F. Qejvanaj, S. Jiang, T. Q. Le, J. Weissenrieder, and J. Åkerman, Low operational current spin Hall nano-oscillators based on NiFe/W bilayers, Appl. Phys. Lett. **109**, 242402 (2016).

[17] X. Fan, J. Wu, Y. Chen, M. J. Jerry, H. Zhang, and J. Q. Xiao, Observation of the nonlocal spin-orbital effective field, Nat. Commun. **4**, 1799 (2013).

[18] L. Liu, C.-F. Pai, Y. Li, H. W. Tseng, D. C. Ralph, and R. A. Buhrman, Spin-torque switching with the giant spin Hall effect of tantalum, Science **336**, 555 (2012).

[19] Y. Fan, P. Upadhyaya, X. Kou, M. Lang, S. Takei, Z. Wang, J. Tang, L. He, L. Chang, M. Montazeri, G. Yu, W. Jiang, T. Nie, R. N. Schwartz, Y. Tserkovnyak, and K. L. Wang, Magnetization switching through giant spin–orbit torque in a magnetically doped topological insulator heterostructure, Nat. Mater. **13**, 699 (2014).

[20] J. C. Rojas- Sánchez, N. Reyren, P. Laczkowski, W. Savero, J. P. Attané, C. Deranlot, M. Jamet, J. M. George, L. Vila, and H. Jaffrès, Spin Pumping and Inverse Spin Hall Effect in Platinum: The Essential Role of Spinmemory Loss at Metallic Interfaces, Phys. Rev. Lett. **112**, 106602 (2014).

[21] Y. Liu, Z. Yuan, R. J. H. Wesselink, A. A. Starikov, and P. J. Kelly, Interface Enhancement of Gilbert Damping from First Principles, Phys. Rev. Lett. **113**, 207202 (2014).

[22] L. Liu, T. Moriyama, D. C. Ralph, and R. A. Buhrman, Spin-Torque Ferromagnetic Resonance Induced by the Spin Hall Effect, Phys. Rev. Lett. **106**, 036601 (2011).

[23] C.-F. Pai, L. Liu, Y. Li, H. W. Tseng, D. C. Ralph, and R. A. Buhrman, Spin transfer torque devices utilizing the giant spin Hall effect of tungsten, Appl. Phys. Lett. **101**, 122404 (2012).

[24] A. R. Mellnik, J. S. Lee, A. Richardella, J. L. Grab, P. J. Mintun, M. H. Fischer, A. Vaezi, A. Manchon, E.-A. Kim, N. Samarth, and D. C. Ralph, Spin-transfer torque generated by a topological insulator, Nature **511**, 449 (2014).

[25] M. Kimata, H. Chen, K. Kondou, S. Sugimoto, P. K. Muduli, M. Ikhlas, Y. Omori, Takahiro Tomita, A. H. MacDonald, S. Nakatsuji, and Y. Otani, Magnetic and magnetic inverse spin Hall effects in a non-collinear antiferromagnet, Nature **565**, 627 (2019).

[26] W. Zhang, W. Han, S. Yang, Y. Sun, Y. Zhang, B. Yan, and S. S. P. Parkin, Giant facet-dependent spin-orbit torque and spin Hall conductivity in the triangular antiferromagnet IrMn3, Sci. Adv. **2**, e1600759 (2016).

[27] W. Zhang, W. Han, X. Jiang, S. Yang, and S. S. P. Parkin, Role of transparency of platinum–ferromagnet interfaces in determining the intrinsic magnitude of the spin Hall effect, Nat. Phys. **11**, 496 (2015).

[28] Z. Tang, B. Wang, H. Yang, X. Xu, Y. Liu, D. Sun, L. Xia, Q. Zhan, B. Chen, M. Tang, Y. Zhou, J. Wang, and R. Li, Magneto-mechanical coupling effect in amorphous $Co_{40}Fe_{40}B_{20}$ films grown on flexible substrates, Appl. Phys. Lett. **105**, 103504 (2014).

[29] D. Fang, H. Kurebayashi, J. Wunderlich, K. Výborný, L. P. Zârbo, R. P. Campion, A. Casiraghi, B. L. Gallagher, T. Jungwirth, and A. J. Ferguson, Spin–orbit-driven ferromagnetic resonance, Nat. Nanotech. **6**, 413 (2011).

[30] C. Kittel, On the theory of ferromagnetic resonance absorption, Phys. Rev. B **73**, 155 (1948).

[31] W. Skowroński, Ł. Karwacki, S. Ziętek, J. Kanak, S. Łazarski, K. Grochot, T. Stobiecki, P. Kuświk, F. Stobiecki, and J. Barnaś, Determination of Spin Hall Angle in Heavy-Metal/Co-Fe-B-Based Heterostructures with Interfacial Spin-Orbit Fields, Phys. Rev. Appl. **11**, 024039 (2019).

[32] C. Guillemard, S. Petit-Watelot, S. Andrieu, and J.-C. Rojas-Sánchez, Charge-spin current conversion in high quality epitaxial Fe/Pt systems: Isotropic spin Hall angle along different in-plane crystalline directions, Appl. Phys. Lett. **113**, 262404 (2018).

[33] K. U. Demasius, T. Phung, W. Zhang, B. P. Hughes, S. H. Yang, A. Kellock, W. Han, A. Pushp, and S. S. P. Parkin, Enhanced spin–orbit torques by oxygen incorporation in tungsten films, Nat. Commun. **7**, 10644 (2016).

[34] S. Woo, M. Mann, A. J. Tan, L. Caretta, and G. S. D. Beach, Enhanced spin-orbit torques in Pt/Co/Ta heterostructures, Appl. Phys. Lett. **105**, 212404 (2014).

[35] H. Saglam, J. C. Rojas-Sanchez, S. Petit, M. Hehn, W. Zhang, J. E. Pearson, S. Mangin, and A. Hoffmann, Independence of spin-orbit torques from the exchange bias direction in $Ni_{81}Fe_{19}$/IrMn bilayers, Phys. Rev. B **98**, 094407 (2018).